Structural insights into the catalytic mechanism of a family 18 exo-chitinase

D. M. F. van Aalten*†, D. Komander*, B. Synstad‡, S. Gåseidnes‡, M. G. Peter§, and V. G. H. Eijsink‡

*Wellcome Trust Biocentre, Department of Biochemistry, University of Dundee, Dundee DD1 5EH, Scotland; ‡Department of Chemistry and Biotechnology, Agricultural University of Norway, Ås N-1432, Norway; and §Institute for Organic Chemistry and Structure Analysis, University of Potsdam, D-14476 Golm, Germany

Edited by Gregory A. Petsko, Brandeis University, Waltham, MA, and approved May 17, 2001 (received for review March 2, 2001)

Chitinase B (ChiB) from *Serratia marcescens* is a family 18 exo-chitinase whose catalytic domain has a TIM-barrel fold with a tunnel-shaped active site. We have solved structures of three ChiB complexes that reveal details of substrate binding, substrate-assisted catalysis, and product displacement. The structure of an inactive ChiB mutant (E144Q) complexed with a pentameric substrate (binding in subsites −2 to +3) shows closure of the ''roof'' of the active site tunnel. It also shows that the sugar in the −1 position is distorted to a boat conformation, thus providing structural evidence in support of a previously proposed catalytic mechanism. The structures of the active enzyme complexed to allosamidin (an analogue of a proposed reaction intermediate) and of the active enzyme soaked with pentameric substrate show events after cleavage of the glycosidic bond. The latter structure shows reopening of the roof of the active site tunnel and enzyme-assisted product displacement in the +1 and +2 sites, allowing a water molecule to approach the reaction center. Catalysis is accompanied by correlated structural changes in the core of the TIM barrel that involve conserved polar residues whose functions were hitherto unknown. These changes simultaneously contribute to stabilization of the reaction intermediate and alternation of the pKa of the catalytic acid during the catalytic cycle.

Chitinases hydrolyze chitin, a linear polymer of β-(1,4)-linked *N*-acetylglucosamine (NAG), which is an abundant biopolymer. These enzymes are essential to chitin-containing organisms (fungi, insects, crustaceans) and are used by several bacteria to exploit chitin as a source of energy. Chitinase inhibitors have generated a lot of interest given their potential as insecticides (1), fungicides (2, 3), and antimalarials (4, 5). Biotechnological exploitation of chitinases, as well as design of inhibitors with sufficiently high selectivity and affinity, requires detailed knowledge of the catalytic mechanism and enzyme-substrate interactions.

Most nonplant chitinases belong to glycosidase family 18 (6) and degrade chitin with retention of the stereochemistry at the anomeric carbon (7–10). The reaction is thought to be initiated by distortion of the −1 sugar ring and protonation of the glycosidic oxygen by a protonated acidic residue. The subsequent nucleophilic attack differs from classical reaction mechanisms of retaining enzymes such as lysozyme (11) and amylases (12) in that it involves the *N*-acetyl group of the −1 sugar, rather than a carboxylate side chain on the protein (8, 9, 13, 14). Thus, the first step of chitinolysis results in cleavage of the sugar chain and formation of an oxazolinium ion intermediate, and hydrolysis of this ion completes the reaction (9, 15) (Fig. 1).

Although the current model for the catalytic mechanism is well established, the amount of structural evidence in its support is limited (8). Important elements of the proposed mechanism were inferred from modeling studies and structures of glycosidases that do not belong to family 18 (9, 15, 16). Furthermore, the model does not account for the roles of several highly conserved residues in family 18 chitinases that are known to be important for catalytic activity (17–19). Substrate binding in the − subsites has been studied in hevamine, a family 18 endochitinase with an open active site architecture (8, 20). However, little is known about substrate binding (and product displacement) in exo-chitinases with complex, tunnel-like active site clefts, such as chitinase B (ChiB) from *Serratia marcescens* (21). We have addressed these issues by solving and studying the crystal structures of several ChiB complexes. ChiB is an exo-chitinase that degrades chitin chains from the nonreducing end by cleaving off NAG_2 or NAG_3 (21, 22). In addition to a catalytic domain with a TIM-barrel fold, ChiB contains a chitin-binding domain that can interact with the reducing end of substrates that extend beyond subsites in the active-site cleft (21).

BIOCHEMISTRY

Methods

ChiB mutants were made by using the QuickChange site-directed mutagenesis kit from Stratagene. The DNA sequences of mutated gene fragments were checked by using an ABI PRISM Dye Terminator Cycle Sequencing Ready Reaction Kit and an ABI PRISM 377 DNA Sequencer (Perkin–Elmer Applied Biosystems), and mutant genes were cloned and overexpressed in *Escherichia coli* as described (22). Catalytic activities were determined by using previously described assays with 4-methylumbelliferyl-β-D-*N*,*N*′-diacetylchitobioside (4MU-NAG_2; an analogue of the natural substrate NAG_3) (22). ChiB variants were purified, characterized, and crystallized as described (21, 22). Crystals (grown at pH 7) of the inactivated mutant Glu-144–Gln (EQ) were cryoprotected through addition of 20% (vol/vol) glycerol, soaked with 25-fold molar excess of NAG_5 (EQ_NAG5), and frozen in a nitrogen stream. An identical procedure was followed for wild type (WT), which was soaked in 25-fold excess allosamidin (WT_ALLO). A cryotrapped reaction intermediate (WT_RX) was obtained by soaking a relatively small WT crystal (approximately $0.1 \times 0.1 \times 0.1$ mm, grown at pH 5.6) in 10% (vol/vol) ethylene glycol together with a 25-fold molar excess of NAG_5 for 30 min, followed by freezing in a nitrogen stream.

Diffraction data (Table 1) were collected at the European Synchrotron Radiation Facility, Grenoble, on beamline ID14–1 (EQ and EQ_NAG5) and at Deutsches Elektronen Synchrotron, Hamburg, on beamlines X11 (WT_ALLO) and X31 (WT_RX). Structures were refined with CNS (23) with different sets of reflections for R_{free} by using the published WT ChiB structure (21) as a template after simulated annealing runs at 2,500 K to remove bias (Table 1). Model building was performed with O (24). Moieties bound to the active site were not included in the model until they could be clearly identified in unbiased $F_o - F_c$ maps (see Fig. 2). The chitin pentamer in EQ_NAG5, allosa-

This paper was submitted directly (Track II) to the PNAS office.

Abbreviations: NAG, *N*-acetylglucosamine; ChiB, chitinase B; WT, wild type.

Data deposition: The atomic coordinates and structure factors have been deposited in the Protein Data Bank, www.rcsb.org (PDB ID codes 1E6P, 1E6N, 1E6R, and 1E6Z).

†To whom reprint requests should be addressed. E-mail: dava@davapc1.bioch.dundee.ac.uk.

The publication costs of this article were defrayed in part by page charge payment. This article must therefore be hereby marked "*advertisement*" in accordance with 18 U.S.C. §1734 solely to indicate this fact.

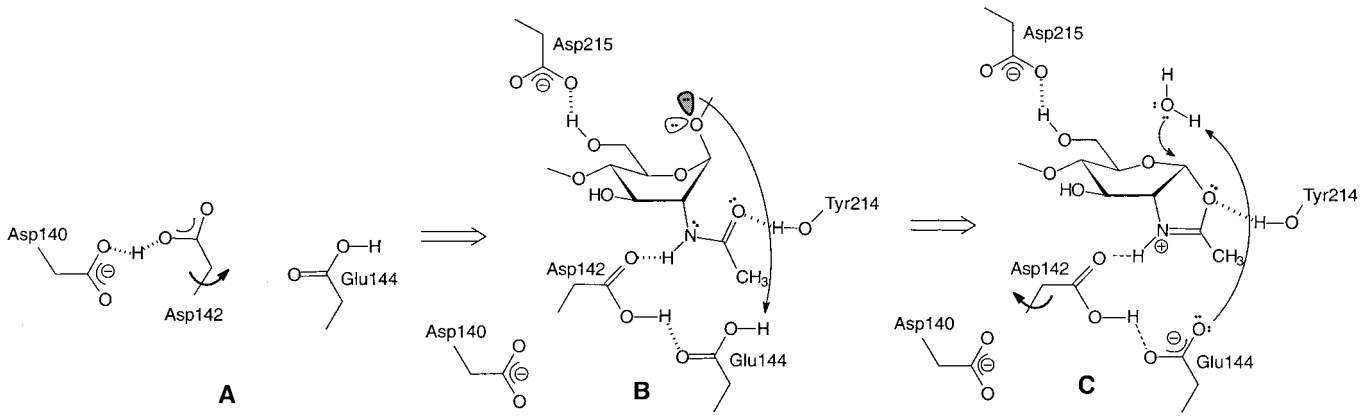

Fig. 1. Proposed catalytic mechanism. Asp-140, Asp-142, and Glu-144, conserved in most family 18 chitinases, are shown during separate stages of catalysis. The mechanism is based on proposals by Tews *et al.* (9) and Brameld and Goddard (15) and refined/expanded on the basis of the results presented in this paper. A three-dimensional view of the changing interactions in the crystal structures described here is shown in Fig. 2. (*A*) Resting enzyme. Asp-142 is too far away to interact with Glu-144. (*B*) Binding of substrate (only −1 binding NAG residue is shown) causes distortion of the pyranose ring to a boat or skewed boat conformation (see also Fig. 2) and rotation of Asp-142 toward Glu-144, enabling hydrogen bond interactions between the hydrogen of the acetamido group, Asp-142, and Glu-144. (*C*) Hydrolysis of the oxazolinium ion intermediate leads to protonation of Glu-144 and rotation of Asp-142 to its original position where it shares a proton with Asp-140.

midin in WT_ALLO, and the dimer bound to the + subsites in WT_RX were built early on in the refinement. Well-ordered density in the −1 subsite in WT_RX appeared during the later stages of refinement (4–9.5 σ peaks). Although the density might be compatible with the structure of an oxazolinium ion intermediate (see Fig. 4), we felt the density was not completely unambiguous and we decided not to refine a model of this putative intermediate. For all structures, some differences were found between the two independent monomers in the asymmetric unit. In the interest of simplicity, differences between the structures described here are discussed by using the same monomer consistently. All images were generated by using BOBSCRIPT (25) and RASTER3D (26).

Results and Discussion

We have solved four crystal structures of a family 18 exochitinase from *S. marcescens* (ChiB, Fig. 2), that approximate different substates along the reaction pathway (Fig. 1). They are referred to as EQ (a 4,000-fold less active mutant in which the catalytic acid Glu-144 is replaced by Gln), EQ_NAG5 (E144Q complexed with an *N*-acetylglucosamine pentamer), WT_ALLO (WT complexed with allosamidin, an inhibitor resembling the putative reaction intermediate; refs. 1, 8, and 9), and WT_RX (a structure solved from a flash-frozen crystal soaked in a solution containing NAG_5).

The structure of EQ (Fig. 2) was refined to 1.7-Å resolution. It represents the highest resolution ChiB structure currently determined and at the same time provides a proper reference frame for interpretation of the EQ_NAG5 structure. The E144Q mutation does not introduce significant changes in the active site or in the overall structure compared with the WT apoenzyme structure published previously (21) (rms deviation on catalytic core Cαs = 0.27 Å).

Table 1. Details of data collection and structure refinement

	EQ	EQ_NAG5	WT_ALLO	WT_RX
Cell dimensions (Å)	*a* = 56.13	*a* = 55.73	*a* = 55.48	*a* = 55.80
	b = 104.14	*b* = 104.48	*b* = 103.43	*b* = 103.81
	c = 186.65	*c* = 186.68	*c* = 185.01	*c* = 186.36
Resolution range (Å)	40–1.7 (1.76–1.7)	40–2.25 (2.33–2.25)	25–2.5 (2.59–2.5)	50–2.0 (2.06–2.0)
No. observed reflections	465,926 (36,964)	123,855 (6,725)	139,537 (13,502)	197,360 (12,216)
No. unique reflections	118,061 (10,746)	47,907 (3,349)	37,616 (3,679)	70,359 (5,320)
Redundancy	3.9 (3.4)	2.6 (2.0)	3.7 (3.7)	2.8 (2.3)
I/σI	13.6 (2.3)	22.6 (4.7)	8.9 (2.9)	9.5 (2.1)
Completeness (%)	97.7 (90.2)	89.8 (63.1)	99.8 (99.9)	92.8 (71.2)
R_{merge} (%)	6.3 (40.0)	4.6 (19.5)	10.9 (42.6)	9.1 (55.9)
R_{cryst} (%)	18.2	18.9	19.8	18.7
R_{free} (%)	22.6	23.9	25.5	22.5
No. R_{free} reflections	1,190	985	774	1,442
No. protein atoms	7,892	7,791	7,780	7,864
No. water molecules	1,113	442	351	934
Refined carbohydrate	None	NAG_5	Allosamidin	NAG_2
rmsd bond ideality (Å)	0.011	0.010	0.007	0.010
rmsd angle ideality (°)	1.6	1.5	1.3	1.5
$\langle B_{prot} \rangle$ (Å^2)	20.0	27.5	22.3	21.4
$\langle B_{carbohydrate} \rangle$ (Å^2)	—	25.4	27.6	31.1

Values between brackets are for the highest resolution shell. Crystals were of space group $P2_12_12_1$, and were cryo-cooled to 100 K. All measured data were included in structure refinement.

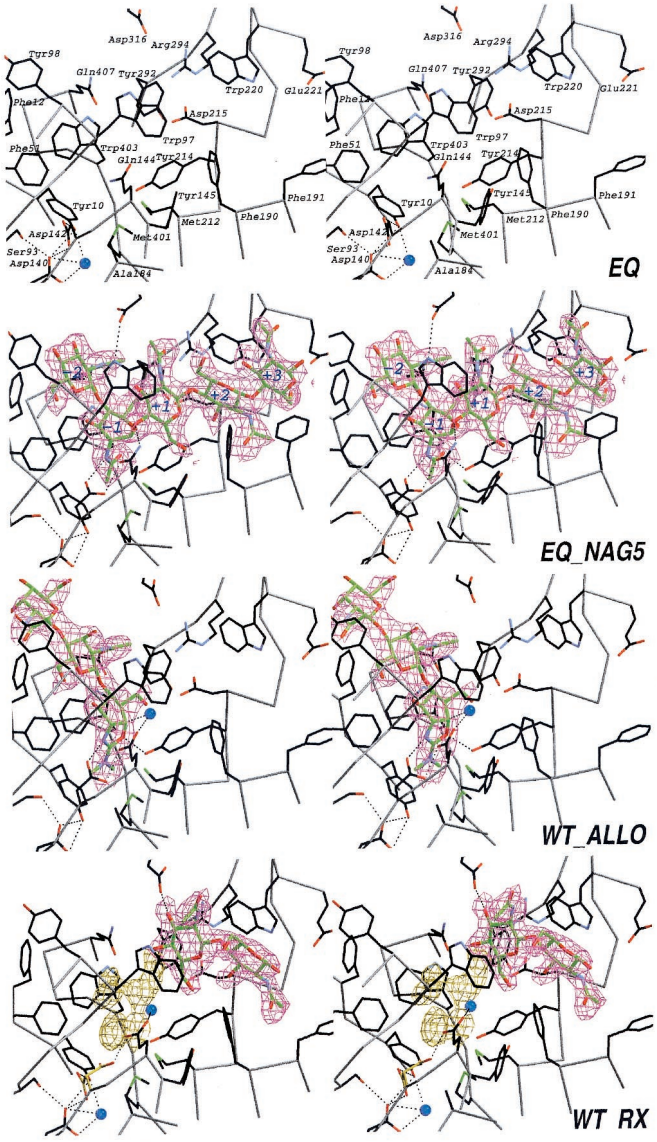

Fig. 2. Structures of the ChiB complexes. The EQ, EQ_NAG5, WT_ALLO, and WT_RX structures are shown as stereo images in the sequence as they would occur along the reaction coordinate (see also Fig. 1). In the stereo images, side chains (carbons in black) interacting with the sugars are shown as sticks, together with relevant stretches of backbone (gray). The sugars are drawn in a stick model with green carbons. Water molecules discussed in the text are shown as blue spheres. Unbiased $F_o - F_c$ maps (i.e., before inclusion of any ligand atom) are contoured at 2.25 σ [magenta, except for the uninterpreted density at −1 in WT_RX (yellow)]. Hydrogen bonds discussed in the text are drawn as dotted lines. Labels identify amino acid side chains in EQ, and the sugars bound to subsites −2 to +3 in EQ_NAG5.

EQ_NAG5 was refined to 2.25-Å resolution and represents the first structure of a chitin oligomer spanning the catalytic site of a multidomain chitinase. NAG_5 binding (in subsites −2 to + 3) results in a number of conformational changes (Fig. 2). Residue 144, whose position is unchanged, lies 3.2 Å from the scissile glycosidic oxygen. Residue Asp-142 rotates −114° around χ_1 such that it no longer interacts with Asp-140, but points with its Oδ1 toward the Oε1 of residue 144 and with Oδ2 toward the hydrogen on the acetamido group of the −1 sugar. Other interactions between the protein and the −1 sugar include hydrogen bonds with Tyr-214 and Asp-215 and hydrophobic contacts with Trp-403. The sugar is in the boat conformation (Fig. 2), providing direct structural evidence for the distortion that was predicted on the basis of a family 20 glycosidase structure (9) and theoretical studies (15). Our EQ_NAG5 structure shows that the *N*-acetyl group is fixed in a conformation in which its oxygen is positioned only 3.0 Å from the anomeric carbon (C1) (Figs. 1 and 2). Consequently, the glycosidic oxygen, i.e., the leaving group, is oriented close to colinear (172°) with the anomeric carbon and the *N*-acetyl oxygen, which is a favorable alignment for nucleophilic attack on C1 (see ref. 27 for an example of such a distortion in another type of glycosidase).

The rotation of Asp-142 upon substrate binding is important not only for stabilizing the developing positive charge of the intermediate oxazolinium ion, but also for donating a proton to and thus lowering the pKa of Glu-144 (Fig. 1). In both the WT (21) and the EQ structure an ordered water molecule is observed at hydrogen-bonding distance of the solvent-exposed Glu-144. Upon substrate binding, water molecules are displaced from the active site and Glu-144 is likely to be protonated (9, 15). Rotation of the protonated Asp-142 stabilizes a deprotonated Glu-144 and thus promotes protonation of the glycosidic oxygen by the latter (Fig. 1). Most interestingly, the change in the Asp-142 conformation is accompanied by structural changes deeper in the core of the TIM barrel that compensate for the loss of the hydrogen bond between Asp-140 and Asp-142 (Figs. 1 and 2). Tyr-10 (and the backbone from residues 9–29) shifts by up to 2 Å, placing its phenolic hydroxyl group at 2.6 Å from Asp-140–Oδ2. As a result, the water molecule originally hydrogen-bonded to Asp-140 is replaced by a more acidic hydrogen bond donor (Fig. 2). In addition, the side chain of Ser-93 moves toward Asp-140, strengthening the hydrogen bond between the two residues and filling the void resulting from the Asp-142 conformational change. These observations shed light on the roles of Tyr-10, Ser-93, and Asp-140, which are conserved in family 18 chitinases but whose functions were hitherto not well understood. The main function of Asp-140 is probably to raise the pKa of Asp-142, whereas Ser-93 and Tyr-10 contribute to catalysis by stabilizing Asp-140 while Asp-142 is in the up position. The importance of Asp-142 in catalysis is further illustrated by the results of mutagenesis studies (B.S., S.G., J. E. Nielsen, D.M.F.v.A., G. Vriend, and V.G.H.E., unpublished data), which show that the basic arm of the pH activity profile of ChiB is not determined by deprotonation of the catalytic acid (E144Q has an unchanged pH activity profile) but rather by deprotonation of Asp-142 (the D142N mutation makes catalysis independent of pH in the experimentally accessible pH range) (Fig. 3*B*). To confirm the proposed roles of Ser-93 and Tyr-10, we constructed the Y10F and S93A mutants, which indeed both displayed a reduction in activity (Fig. 3*B*). Interestingly, the pH activity profile of the S93A mutant is similar to that of D142N (Fig. 3*B*), supporting the notion that the catalytic role of the proton on Asp-142 is coupled to the presence of Ser-93. Replacing Tyr-10 by phenylalanine yielded a similar decrease in activity as for the S93A mutant (Fig. 3*B*, the basic arm of the pH activity profile for Y10F could not be determined because of enzyme instability).

Binding of substrate induces several other conformational changes that result in favorable protein-substrate interactions. Trp-97 and Trp-220 move 1.0 Å toward each other, creating a hydrophobic sandwich with the sugars at the +1 and +2 positions (Figs. 2 and 3). Asp-316 rotates 152° around χ_1, leading to formation of a hydrogen bond with Trp-97 on the opposite side of the substrate. Together, these movements lead to partial closure of the roof of the active site tunnel (Fig. 3). Another notable change is the rotation of −91° around Phe-190 χ_1, which results in a hydrophobic interaction with the sugar at +3 (Figs. 2 and 3). These phenomena of induced fit and loop closure upon substrate binding are not uncommon in glycosidases acting on other polymeric substrates such as, for example, cellulose (28–30). It is further worth noting that although the NAG_5 substrate

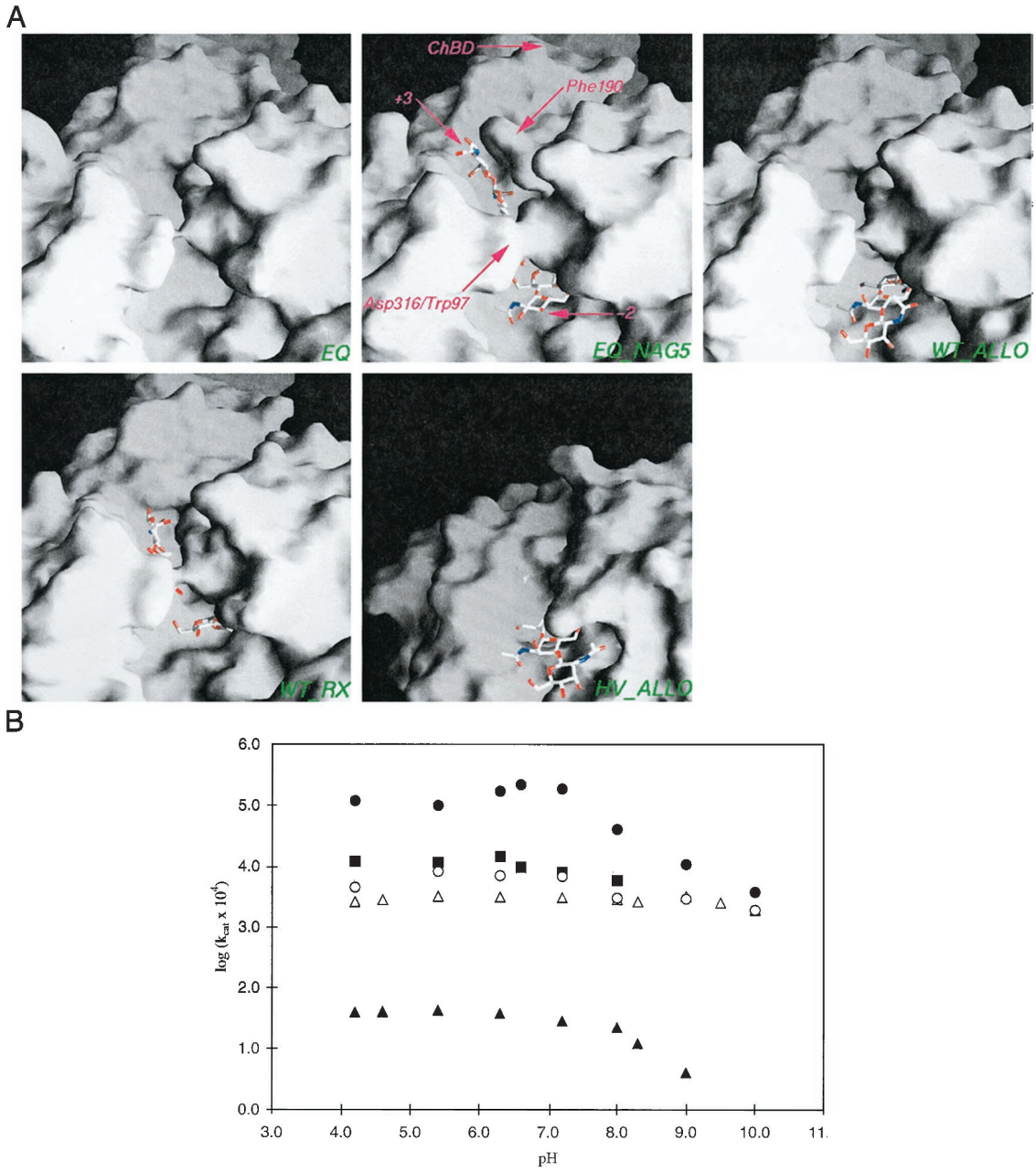

Fig. 3. (*A*) Molecular surface representations (calculated with GRASP, ref. 37) are shown for the four structures described here, and also for the structure of hevamine in complex with allosamidin (8). The carbohydrate moieties are shown in a stick representation, including a model for the putatative oxazolinium ion intermediate in WT_RX. Note the more open active site of hevamine, compared with the tunnel-like active site of ChiB. In the EQ_NAG5 structure, arrows have been added to highlight features discussed in the text: the flip of Phe-190, the tunnel formed by residues Asp-316/Trp-97, the sugar binding subsites (+3, −2), and the chitin binding domain (ChBD). (*B*) pH activity profiles of WT ChiB (●) and the E144Q (▲), D142N (△), S93A (○), and Y10F (■) variants. A detailed mutational analysis of acidic residues in the active site of ChiB will be published elsewhere.

used for the EQ_NAG5 complex does not reach the chitin binding domain, this domain refines to somewhat different positions in the complexes described here (for instance, EQ_NAG5 vs. EQ, 6.5° change in the angle between the chitin binding and the catalytic domains, with backbone shifts of up to 3.2 Å).

Allosamidin is a natural pseudotrisaccharide inhibitor of family 18 chitinases (1, 31) and binds to subsites −3 to −1 in our 2.5-Å structure (Fig. 2) and in a complex with hevamine (8). The unit binding in subsite −1 is the pseudosugar allosamizoline that resembles the proposed oxazolinium ion intermediate in ChiB formed after nucleophilic attack of the *N*-acetyl group of the −1 sugar on the anomeric carbon (8) (Fig. 1). Binding of allosamidin to WT ChiB results in similar structural changes as binding of NAG_5 to the E144Q mutant (Fig. 2): Asp-142 is in the up position and interacts with the positive charge in the oxazolinium ion, whereas Asp-140 is compensated for the loss of the interaction with Asp-142 by structural adjustments of Tyr-10 and Ser-93. A notable difference between EQ_NAG5 and WT_ALLO is the appearance of a well-ordered water molecule (*B* factor 19.4 $Å^2$) at 3.3 Å from the C1 carbon in the allosamizoline ring. This water molecule is coordinated by interactions with Glu-144–Oε1 (2.6 Å) and two water molecules (3.2/2.7 Å), which themselves are tightly bound in the active site (not shown

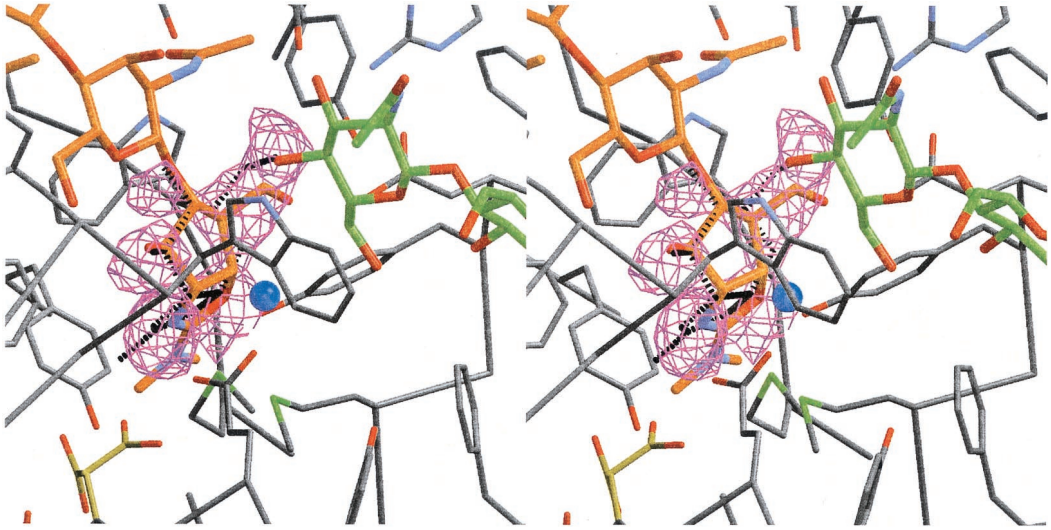

Fig. 4. Details of the WT_RX density. The details of the active site in the WT_RX stucture are shown together with the displaced NAG dimer (green carbons) and the position taken up by allosamidin in the WT_ALLO structure (orange carbons). The unbiased $F_o - F_c$ map (i.e., before inclusion of any ligand atom) contoured at 2.25 σ (magenta) is shown for the -1 position, as well as a model for the putative oxazolinium ion intermediate (black dashed lines). The putative catalytic water molecule is shown as a blue sphere. The two positions for Asp-142 are also shown (yellow carbons).

in Fig. 2). We note that the same water molecule is present in the structure of the hevamine-allosamidin complex (8) (PDB entry 1LLO), although this has not been discussed previously (the water molecules in the ChiB-allosamidin and hevamine-allosamidin complexes are within 0.5 Å from each other after superposition of the oxazoline moieties). The water molecule in WT_ALLO has approximately the same location as the glycosidic oxygen in EQ_NAG5. If an oxazolinium ion intermediate would bind at a position equivalent to the allosamizoline moiety of allosamidin, the attacking group (the water molecule) and the leaving group (the O7 oxygen) would lie on opposite sides of the atom corresponding to the C1 anomeric carbon, at an angle of ≈135°. Such an arrangement would result in hydrolysis of the oxazolinium ion with overall retention of stereochemistry at the C1 carbon.

Our structure represents an example of allosamidin bound in a "tunnel" exo-chitinase, where more side chains interact with the inhibitor than in the endochitinase hevamine, which has a more open architecture (8) (Fig. 3). The affinity of allosamidin for tunnel-like chitinases is an order of magnitude higher than for hevamine (32), and it is thus essential to evaluate the structural determinants of the interaction of an enzyme like ChiB with this potent natural inhibitor. It is worth noting that allosamidin itself was recently shown to be a candidate for a malaria transmission blocker, where it acts on a presumably tunnel-like chitinase homologous to ChiB (4). The structure of allosamidin bound to an exo-chitinase is a useful starting point for structural evaluation of the many allosamidin derivatives that have been developed for chitinase inhibition (e.g., refs. 33 and 34). An evaluation of these compounds in the context of the WT_ALLO structure could provide new leads for structure-based design of inhibitors against chitinases from human pathogens with a ChiB-like active site architecture (3–5, 35).

The WT_RX structure, collected from NAG_5-soaked, flash-frozen crystals and refined to 2.0-Å resolution, appears to represent a view of the WT enzyme during hydrolysis of a natural substrate, NAG_5. The $F_o - F_c$ electron density map calculated before inclusion of any ligand atom, initially revealed two of the five possible sugar rings [Fig. 2; note that cleavage of NAG_5 yields NAG_2 and NAG_3 and that ChiB further degrades the latter to NAG_2 and NAG (22), thus $NAG_{1,\ 2,3,\ 5}$ oligomers may occur in the crystals]. Additional strong density (4–9.5 σ peaks) visible in the -1 subsite in an unbiased $F_o - F_c$ map showed good overlap with the position for the allosamizoline group in the WT_ALLO structure (Fig. 4). This density could represent an intermediate during hydrolysis of NAG_3 initially bound in subsites -1 to $+2$. The density in the -1 subsite is ambiguous (Figs. 2 and 4), but the notion that this density represents carbohydrate is supported by the conformation of Asp-142, which is ≈50% in the down position (pointing toward Asp-140) position and 50% in the up position (pointing toward Glu-144) (Fig. 2). In all family 18 chitinase apo-structures presently available, and also in our high-resolution EQ structure (Fig. 2), Asp-142 points down toward Asp-140 to form a hydrogen bond (3, 20, 21, 36). In all presently known chitinase complex structures, however, Asp-142 is pointing up toward Glu-144 and the *N*-acetyl group as observed in the EQ_NAG5 and WT_ALLO structures described here (Fig. 2; ref. 8, and D.M.F.v.A., G. Kolstad, D.K., and V.G.H.E., unpublished work). Thus, the fact that Asp-142 is partially in the up position in the WT_RX structure agrees with a carbohydrate moiety (partially) occupying the -1 position.

The EQ_NAG5 structure shows that there is no room for a catalytic water molecule near the anomeric carbon as long as the $+1$ subsite is occupied by a sugar residue (Fig. 2). Thus, after the initial catalytic step leading to formation of the oxazolinium ion, one would expect a rearrangement of the chitin chain on the reducing (+) end of cleaved glycosidic bond. Such a rearrangement is indeed observed in WT_RX: the structure shows a well-ordered NAG dimer (average *B* factor 23.5 Å^2), presumably a product of chitinolysis (Fig. 1), that is shifted by up to 4.0 Å and tilted compared with the pentamer in EQ_NAG5, such that the two sugars occupy positions in between $+1/+2$ and $+2/+3$, respectively (Fig. 2). The enzyme seems to contribute actively to the displacement, in particular through interactions between the sugar and Asp-316 in one of the two flexible loops that make up the roof in the active site tunnel (Fig. 2). Comparison of WT_RX with EQ_NAG5 (Fig. 2) shows that the side chain of Asp-316 has rotated 126° around χ_1, thus breaking its interaction with Trp-97, and forming a new hydrogen bond with O3 on the $+1$ sugar. As a result, the "closure" of the active site cleft that occurs upon substrate binding (compare EQ with EQ_NAG5; Fig. 2; see above) is reversed and the $+1$ sugar is tilted away from the $+1$ subsite (see WT_RX; Fig. 2).

The WT_RX structure reveals a well-ordered water molecule (*B* factor 21.0 Å^2) at a similar position as the water molecule

close to C1 in the WT_ALLO structure (Figs. 2 and 4). In an oxazolinium ion reaction intermediate, the anomeric carbon is positively polarized due to the electron withdrawing effect of the oxazolinium ring. As discussed above, the position of this water molecule, which is polarized by Glu-144 and fixed by two other water-mediated hydrogen bonds to the protein, favors nucleophilic attack on the anomeric carbon C1, with overall retention of β-anomeric stereochemistry (Fig. 1).

Concluding Remarks

The present structures provide insight in binding and displacement of substrates and products in the tunnel-like active site of a two-domain exo-chitinase. They also provide structural evidence for and deeper insight into the catalytic mechanism. We provide structural evidence for the hypothesis that substrate binding leads to distortion of the sugar and show that the distorted conformation is closer to a boat than to e.g. a 4-sofa (9, 15), thus optimizing conditions for nucleophilic attack by the *N*-acetyl oxygen. The structures also show how larger parts of the enzyme function together both in relation to interactions with the sugars and in relation to catalysis. The data reveal that residues in the core of the catalytic TIM barrel (Tyr-10, Ser-93, Asp-140) are conserved in most family 18 chitinases because they participate in a system for dispersion of charge and displacement of protons during catalysis.

We thank the European Molecular Biology Laboratory-Hamburg outstation at Deutsches Elektronen Synchrotron, Hamburg, for use of beamlines X11 and X31, and the European Synchrotron Radiation Facility, Grenoble, for the time at beamline ID14–1. We are grateful to Graham Gooday for a sample of allosamidin, Gustav Kolstad for help in refining the WT_ALLO structure, and Ana Maria Fernandez Escamilla for assistance with purification of EQ. D.M.F.v.A. is supported by a Wellcome Trust Career Development Research Fellowship. This work was supported by European Union Grant BIO4-CT-960670.

1. Sakuda, S., Isogai, A., Matsumoto, S. & Suzuki, A. (1987) *J. Antibiot.* **40,** 296–300.
2. Sandor, E., Pusztahelyi, T., Karaffa, L., Karanyi, Z., Pocsi, I., Biro, S., Szentirmai, A. & Pocsi, I. (1998) *FEMS Microbiol. Lett.* **164,** 231–236.
3. Hollis, T., Mozingo, A. F., Bortone, K., Ernst, S., Cox, R. & Robertus, J. D. (2000) *Protein Sci.* **9,** 544–551.
4. Vinetz, J. M., Dave, S. K., Specht, C. A., Brameld, K. A., Xu, B., Hayward, R. & Fidock, D. A. (1999) *Proc. Natl. Acad. Sci. USA* **96,** 14061–14066.
5. Vinetz, J. M., Valenzuela, J. G., Specht, C. A., Aravind, L., Langer, R. C., Ribeiro, J. M. C. & Kaslow, D. C. (2000) *J. Biol. Chem.* **275,** 10331–10341.
6. Henrissat, B. & Davies, G. (1997) *Curr. Opin. Struct. Biol.* **7,** 637–644.
7. Armand, S., Tomita, H., Heyraud, A., Gey, C., Watanabe, T. & Henrissat, B. (1994) *FEBS Lett.* **343,** 177–180.
8. Terwisscha van Scheltinga, A. C., Armand, S., Kalk, K. H., Isogai, A., Henrissat, B. & Dijkstra, B. W. (1995) *Biochemistry* **34,** 15619–15623.
9. Tews, I., Terwisscha van Scheltinga, A. C., Perrakis, A., Wilson, K. S. & Dijkstra, B. W. (1997) *J. Am. Chem. Soc.* **119,** 7954–7959.
10. Honda, Y., Tanimori, S., Kirihata, M., Kaneko, S., Tokuyasu, K., Hashimoto, M., Watanabe, T. & Fukamizo, T. (2000) *FEBS Lett.* **476,** 194–197.
11. Davies, G. J., Mackenzie, L., Varrot, A., Dauter, M., Brzozowski, A. M., Schulein, M. & Withers, S. G. (1998) *Biochemistry* **37,** 11707–11713.
12. Uitdehaag, J. C. M., Mosi, R., Kalk, K. H., van der Veen, B. A., Dijkhuizen, L., Withers, S. G. & Dijkstra, B. W. (1999) *Nat. Struct. Biol.* **6,** 432–436.
13. Knapp, S., Vocadlo, D., Gao, Z., Kirk, B., Lou, J. & Withers, S. G. (1996) *J. Am. Chem. Soc.* **118,** 6804–6805.
14. Kobayashi, S., Kiyosada, T. & Shoda, S. (1996) *J. Am. Chem. Soc.* **118,** 13113–13114.
15. Brameld, K. A. & Goddard, W. A. (1998) *J. Am. Chem. Soc.* **120,** 3571–3580.
16. Tews, I., Perrakis, A., Oppenheim, A., Dauter, Z., Wilson, K. S. & Vorgias, C. E. (1996) *Nat. Struct. Biol.* **3,** 638–648.
17. Watanabe, T., Kobori, K., Miyashita, K., Fujii, T., Sakai, H., Uchida, M. & Tanaka, H. (1993) *J. Biol. Chem.* **268,** 18567–18572.
18. Watanabe, T., Ito, Y., Yamada, T., Hashimoto, M., Sekine, S. & Tanaka, H. (1994) *J. Bacteriol.* **176,** 4465–4472.
19. Tsujibo, H., Orikoshi, H., Imada, C., Okami, Y., Miyamoto, K. & Inamori, Y. (1993) *Biosci. Biotechnol. Biochem.* **57,** 1396–1397.
20. Terwisscha van Scheltinga, A. C., Kalk, K. H., Beintema, J. J. & Dijkstra, B. W. (1994) *Structure (London)* **2,** 1181–1189.
21. van Aalten, D. M. F., Synstad, B., Brurberg, M. B., Hough, E., Riise, B. W., Eijsink, V. G. H. & Wierenga, R. K. (2000) *Proc. Natl. Acad. Sci. USA* **97,** 5842–5847.
22. Brurberg, M. B., Nes, I. F. & Eijsink, V. G. H. (1996) *Microbiology* **142,** 1581–1589.
23. Brunger, A. T., Adams, P. D., Clore, G. M., Gros, P., Grosse-Kunstleve, R. W., Jiang, J.-S., Kuszewski, J., Nilges, M., Pannu, N. S., Read, R. J., *et al*. (1998) *Acta Crystallogr. D* **54,** 905–921.
24. Jones, T. A., Zou, J. Y., Cowan, S. W. & Kjeldgaard, M. (1991) *Acta Crystallogr. A* **47,** 110–119.
25. Esnouf, R. M. (1997) *J. Mol. Graphics* **15,** 132–134.
26. Merritt, E. A. & Murphy, M. E. P. (1994) *Acta Crystallogr. D* **50,** 869–873.
27. Schulzenbacher, G., Driguez, H., Henrissat, B., Schuelein, M. & Davies, G. J. (1996) *Biochemistry* **35,** 15280–15287.
28. Sakon, J., Irwin, D., Wilson, D. B. & Karplus, P. A. (1997) *Nat. Struct. Biol.* **4,** 810–818.
29. Zou, J., Kleijwegt, G. J., Stahlberg, J., Driguez, H., Nerinckx, W., Claeyssens, M., Koivola, A., Teeri, T. T. & Jones, T. A. (1999) *Structure (London)* **7,** 1035–1045.
30. Varrot, A., Schuelein, M. & Davies, G. J. (2000) *J. Mol. Biol.* **297,** 819–828.
31. Sakuda, S., Isogai, A., Matsumoto, S., Suzuki, A. & Koseki, K. (1986) *Tetrahedron Lett.* **27,** 2475–2478.
32. Bokma, E., Barends, T., Terwisscha van Scheltinga, A. C., Dijkstra, B. W. & Beintema, J. J. (2000) *FEBS Lett.* **478,** 119–122.
33. Spindler-Barth, M., Blattner, R., Vorgias, C. E. & Spindler, K. D. (1998) *Pest. Sci.* **52,** 47–52.
34. Berecibar, A., Grandjean, C. & Siriwardena, A. (1999) *Chem. Rev.* **99,** 779–844.
35. Shakarian, A. M. & Dwyer, D. M. (1998) *Gene* **208,** 315–322.
36. Perrakis, A., Tews, I., Dauter, Z., Oppenheim, A. B., Chet, I., Wilson, K. S. & Vorgias, C. E. (1994) *Structure (London)* **2,** 1169–1180.
37. Nicholls, A., Sharp, K. & Honig, B. (1991) *Proteins* **11,** 281–296.